

# To be or not to be oblate: the shape of the dark matter halo in the polar ring galaxies.

S.A. Khoperskov<sup>1,2\*</sup>, A.V. Moiseev<sup>3,2</sup>, A.V. Khoperskov<sup>4</sup>, A.S. Saburova<sup>2</sup>

<sup>1</sup>*Institute of Astronomy, Russian Academy of Sciences†, Pyatnitskaya st., 48, 119017 Moscow, Russia*

<sup>2</sup>*Sternberg Astronomical Institute, Moscow M.V. Lomonosov State University, Universitetskij pr., 13, 119992 Moscow, Russia*

<sup>3</sup>*Special Astrophysical Observatory, Russian Academy of Sciences, 369167 Nizhnii Arkhyz, Karachaevo-Cherkesskaya Republic, Russia*

<sup>4</sup>*Volgograd State University, Universitetsky pr., 100, 400062 Volgograd, Russia*

## ABSTRACT

With the aim to determine the spatial distribution of the dark matter halo, we investigate two polar ring galaxies NGC 4262 and SPRC-7. For both galaxies the stellar kinematics data for the central galaxy were obtained from optical spectroscopy at the 6-m telescope of the Special Astrophysical Observatory of the Russian Academy of Sciences. The information about polar gaseous components was taken from the optical 3D-spectroscopic observations of ionized gas (for SPRC-7) and H I radio observations (for NGC 4262). SPRC-7 is the system with a relative angle  $\delta = 73^\circ$  towards the central galaxy and a quite massive stellar-gaseous polar component. Meanwhile NGC 4262 is the classic polar case with  $\delta = 88^\circ$  where the polar ring mainly consists of neutral gas with a negligible stellar contribution to the mass. We are hence dealing with two different systems and the results are quite diverse too. The observed properties of both galaxies were compared with the results of self consistent simulations of velocity fields of the polar component along with the rotation curve of the central lenticular galaxy. For SPRC-7 we have found a slightly flattened halo towards the polar plane with the axis ratio  $c/a \simeq 1.7 \pm 0.2$  for the isothermal halo model and  $c/a \simeq 1.5 \pm 0.2$  for the NFW model. The case of NGC 4262 is more unusual, the shape of the dark matter distribution varies strongly with radius. Namely, the dark matter halo is fattened in the vicinity of the galactic disc ( $c/a \approx 0.4 \pm 0.1$ ), however it is prolate far beyond the central galaxy ( $c/a \approx 1.7$  for the isothermal halo and  $c/a \approx 2.3$  for NFW).

**Key words:** Galaxies: evolution; galaxies: haloes; galaxies: kinematics and dynamics;

## 1 INTRODUCTION

Following the  $\Lambda$ CDM model, dark matter (DM) is a crucial factor of evolution on the spatial scales of galactic clusters and large-scale structure of the entire Universe. The role of DM in the dynamics and evolution of individual galaxies is much less clear. However, the presence of dark matter haloes around the galaxies is obvious. The long-term stability of galactic discs is supported by the presence of a massive collisionless spheroidal component (Bosma 1981; Begeman et al. 1991; Martinsson et al. 2013). The low ratio of the radial velocity dispersion  $\sigma_r$  to the maximum disc rotation velocity  $V_{\max}$  also indicates the existence of the massive halo (Khoperskov, Zasov & Tyurina 2003). The evolution and lifetime of galactic bars strongly depends on the interaction with the dark matter halo (Sellwood

2006; Sellwood & Debattista 2006; Athanassoula 2013; Athanassoula et al. 2013). Dark matter influences the dynamics of tidal streams in our Galaxy (Ibata et al. 2001; Helmi 2004; Belokurov et al. 2014) and dwarf satellites. The thickness of the stellar disc closely depends on the disc-to-halo mass ratio (Zasov, Makarov & Mikhailova 1991; Khoperskov, Bizyaev, Tiurina & Butenko 2010; Rodionov & Sotnikova 2013), moreover, the observed vertical equilibrium is explained by the presence of a massive DM halo. The investigation of the gaseous and stellar kinematics allows to estimate the total amount of DM mass and its spatial distribution inside the galaxies and their neighbourhood. The measured kinematics of the the Milky Way thick disc stars allows to conclude that the volume density of the dark matter in the Solar vicinity is insignificant (Garbari, Read & Lake 2011).

Triaxiality of dark matter haloes is confirmed owing to the observations of various galactic systems: anisotropy of weak-lensing signals (van Uitert et al. 2012; Strigari 2013), dynamics of hypervelocity of stars (Gnedin et al.

\* khoperskov@inasan.ru

† The system of Russian Academy of Sciences institutes was liquidated on Sep 2013

2005), flaring of the gas layer (Olling & Merrifield 2000), gravitational lensing (Natarajan & Refregier 2000) and so on. The shapes of the X-ray isophotes for the some elliptic galaxies pointed out the manifestation of a triaxial dark matter halo (Buote et al. 2002). Dynamical features of the Sagittarius Stellar Tidal Stream in our Galaxy might be explained by the triaxial dark matter distribution (Law, Majewski & Johnston 2009; Debattista, Roškar, Valluri, Quinn, Moore & Wadsley 2013). It is believed that galactic warps are usually formed and maintained within the triaxial DM haloes (Dubinski & Kuijken 1995; Shen & Sellwood 2006). It was also shown that the nonstationarity of the galactic spiral pattern rotation might be the result of interactions with a non-axisymmetric dark matter halo (Khoperskov et al. 2013; Valenzuela et al. 2013). From the theoretical point of view, the triaxial halo shape is supported, by numerous cosmological simulations which demonstrate the formation of DM halos with different spatial scales  $a \neq b \neq c$  at almost any condition (Dubinski & Carlberg 1991; Jing & Suto 2002; Bailin & Steinmetz 2005; Allgood et al. 2006; Kuhlen et al. 2007; Abadi et al. 2010).

Galaxies having polar rings are among the most ambitious candidates for the measurements of the DM halo shape. This is a type of peculiar objects, characterized by two kinematically decoupled components: a host (or central) galaxy and a polar component (disc or ring), rotating in different planes (see the Fig. 1). The first catalogue, containing 157 PRG candidates and related objects was created by Whitmore et al. (1990). Recently, more than two hundred galaxies with polar rings were found in the SDSS (Moiseev et al. 2011), some of which have a kinematic confirmation. It was believed that polar structures are the result of a close interaction of galaxies (Whitmore et al. 1990; Snaith et al. 2012), accretion of companion's matter (Reshetnikov & Sotnikova 1997) or infalls of cold gaseous filaments (Stanonik et al. 2009; Spavone et al. 2010). In any case, this kind of multi-spin galaxies is a good tool to study the dark and baryonic matter gravitational potential around them. Central galaxies of PRGs are mainly represented by the S0 or elliptical galaxies, which indicates the absence of a significant amount of gas inside of them. Statistical investigation of PRGs revealed a small amount ( $\approx 6\%$ ) of inclined systems (Smirnova & Moiseev 2013). This fact proves that polar (or closely resembling) structures should be stabilized by the gravitational potential of the halo.

It should be noted that the internal structure of PRGs is poorly studied. There are some proofs of ongoing star formation within the gaseous ring (Reshetnikov, Hagen-Thorn & Yakovleva 1994). Non-axisymmetric perturbations from the central galaxies (similar to bar-like perturbations in the discs of galaxies) and self gravity for massive polar rings should lead to the formation of spiral structures (Theis, Sparke & Gallagher 2006). The large-scale non-axisymmetric halo potential is an effective generator of spiral structures in the gaseous component (Bekki & Freeman 2002; Khoperskov et al. 2012). However, there is no satisfactory observational evidence of these substructures in PRGs.

The most well-studied PRG is NGC 4650A. During numerous studies the understanding of DM halo shape in this galaxy has significantly evolved. The first halo shape esti-

mates were done via the comparison of maximal velocities of the central galaxy (hereinafter denoted as CG) and the polar component (Whitmore et al. 1987). This method allows to establish the oblate DM halo shape towards the galactic plane with the halo semi-axis relation  $c/a \sim 0.83 \pm 0.21$ .

The position of polar ring galaxies on the Tully-Fisher diagram allows us to estimate the deviations of the gravitational potential from the spherical shape. The majority of PRGs do not follow the main relation for the spiral galaxies in the Tully-Fisher diagram because they are shifted to larger rotation velocities (Iodice, Arnaboldi, Bournaud, Combes, Sparke, van Driel & Capaccioli 2003; Reshetnikov 2004; Combes, Moiseev & Reshetnikov 2013). A comparison with the model galaxies reveals an oblate DM halo towards the polar plane (Iodice et al. 2008; Iodice 2010).

A kinematic model based on the variations of the  $M/L$  ratio and halo flattening provides the constrains on the dark halo shape in NGC 4650A (Sackett & Sparke 1990). If the ring is not massive, the DM halo is non-spherical, however, the halo shape varies in the range of E0-E6 (halo flattened towards the polar plane). Another kinematic model by Combes & Arnaboldi (1996) also argues that the dark halo of the polar ring galaxy NGC 4650A is flattened towards the polar ring plane. Nevertheless, despite the differences in the estimated shape of the DM halo, an important argument in favour of the flattened halo in the PRG (in the plane of the galaxy) is the stability of polar orbits for such a kind of configuration of the gravitational potential (Steiman-Cameron & Durisen 1982; Wakamatsu 1993).

A surprising feature of DM distribution was found in the simulations of the formation of PRGs due to major merging. Snaith et al. (2012) showed that the major and minor halo axes are swapped along the radius. In fact, this means a change of the type of the halo shape. In the central part the halo could be flattened to the plane of the central galaxy, but beyond the optical radius of the galaxy it becomes flattened to the polar plane. Thus, within this framework it is possible to combine the accumulated knowledge about the NGC 4650A halo parameters. Nevertheless, there are no observations in favour of such kind of dark matter distribution yet.

Formally, there are no observational (or theoretical) evidences confirming that the PRG assembly strongly differs from regular galaxies. If it is true, the DM halo structure is expected to be similar. However, the resulting baryonic objects are not similar. Of course, dark matter plays the dominant role in the formation of galaxies. This means that the current galaxy type depends on the abundance of gas (and/or stars) inside the merging DM haloes at  $z > 0$ . Perhaps it is possible to form various galaxies within the given DM haloes assembly process. On another hand, the DM halo shape in the cosmological context is not constant in time tending to the more spherical shape at smaller redshifts (e.g. see Allgood et al. 2006). As it was mentioned above, polar rings around the galaxies are usually more stable in non-spherical haloes. Thus, the proper evolution of DM haloes should destroy the polar components. Thus, PRGs haloes have another structure, than the DM around regular galaxies because it is related to another epoch of evolution. However, the mutual influence of the DM halo and the baryonic fraction could complicate these submission. We are not sure

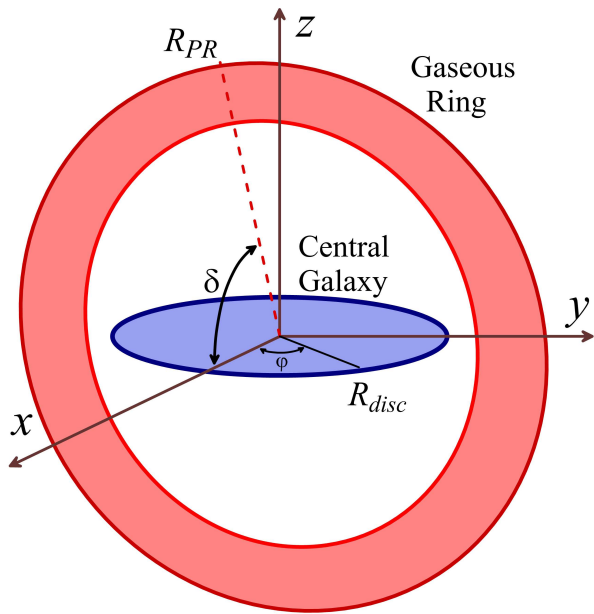


**Figure 1.** Scheme of spatial orientation of the components in a polar ring galaxy. We placed the central lenticular galaxy for both PRGs in the XY-plane. A gaseous ring is situated in the YZ-plane in the classic polar case for NGC 4262 —  $\delta = 88^\circ$ . The ring plane in SPRC-7 is inclined towards the XY-plane at the angle  $\delta = 73^\circ$ .

now that the conclusions about the DM halo shape of PRGs could be directly applied to the regular galaxies.

In this paper we present the observations of two PRGs together with the study of the spatial distribution of dark matter. The following observations were used: the long-slit spectral data of the central galaxies NGC 4262 and SPRC-7 obtained at the 6-m telescope of the Special Astrophysical Observatory of the Russian Academy of Sciences (SAO RAS); 21 cm H I observations of the ring in NGC 4262 (Oosterloo et al. 2010); the scanning Fabry-Perot interferometric H $\beta$  observations of ionized gas in the ring of SPRC-7 (Finkelmann et al. 2011). The halo shape determination is based on the detailed decomposition of the baryon matter rotation in different planes, namely, the stellar discs in central galaxies and the gaseous rings. Our paper is organized as follows: Section 2 describes the observations of both galaxies. Section 3 presents the model of the galactic potential, basic parameters of the system and the fitting procedure. Basic results are presented in Section 4.

## 2 OBSERVATIONAL DATA

### 2.1 Long-slit spectral observations

The spectroscopic observations at the prime focus of the SAO RAS 6-m telescope were made with the SCORPIO multi-mode focal reducer (Afanasiev & Moiseev 2005) and its new version SCORPIO-2 (Afanasiev & Moiseev 2011). When operated in the long-slit mode, both devices have the same slit, 6.1 arcmin in height, with a scale of 0.36 arcsec per pixel. However, with a similar spectral resolution SCORPIO-2 provides a twice larger spectral range. The CCDs employed

were the EEV 42-40 in the SCORPIO and E2V 42-90 in the SCORPIO-2.

Table 1 gives the log of observations: position angles of the spectrograph slit for each galaxy, observing date, slit width, spectral range, spectral resolution (estimated by the mean FWHM of airglow lines), total exposure, and seeing. The data reduction was made in a standard way using the IDL-based software package developed at the SAO RAS (Afanasiev & Moiseev 2005). The measurements of the distribution of the line-of-sight velocities and stellar velocity dispersion were carried out by cross-correlating the spectra of galaxies with the spectra of the template star observed on the same nights. The measurement technique has already been described in our previous papers (Moiseev 2001; Moiseev et al. 2011). Figure 2 shows the line-of-sight velocity and velocity dispersion distributions for each slit position.

### 2.2 SPRC 7

The polar structure in this galaxy has been discovered and described in the paper by Brosch et al. (2010) based on the SDSS images and 6-m telescope spectroscopic data. On the optical images the galaxy appears as a giant counterpart of NGC 4650A because the central early-type galaxy is surrounded by a large ring with a significant contribution of young stars. In contrast to NGC 4650A, the SPRC 7 galaxy is more distant (about 40 kpc in diameter) and moderately inclined. The external structure is more likely to be a ‘polar disc’ than a ring, the total luminosity in the  $g$ -band is even larger than for the central galaxy. The accepted distance for the galaxy is  $D = 233$  Mpc, the scale is 1.13 kpc per arcsec.

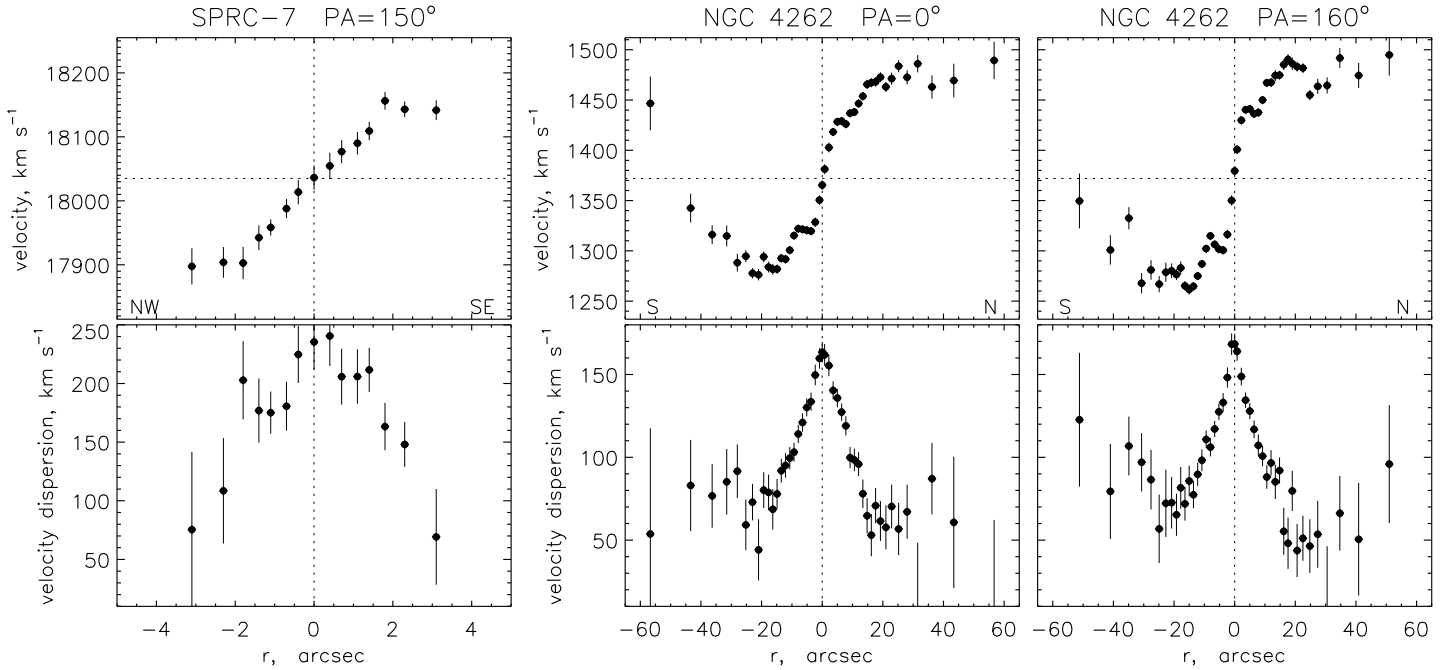
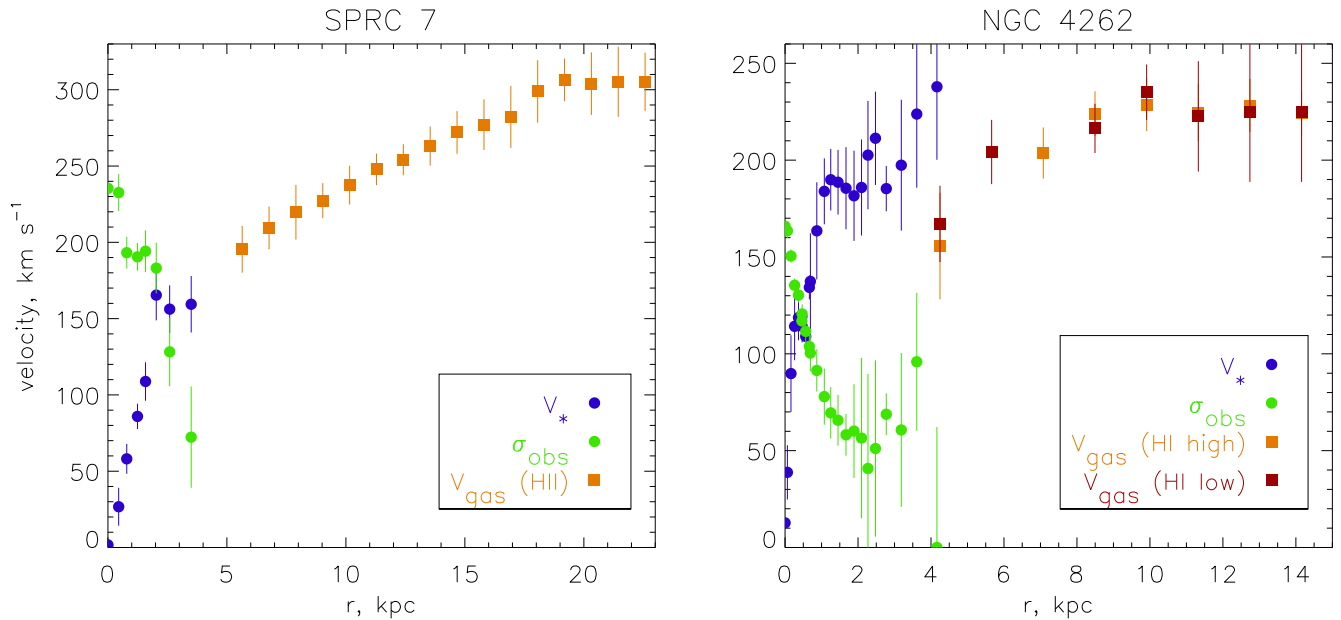
Our long-slit spectra were taken along the photometric major axis of the CG. The new measurements of the stellar kinematics parameters show a significantly smaller scatter compared with data presented in Brosch et al. (2010). The line-of-sight velocities, as well as stellar velocity dispersion have a symmetric distribution relative to the galaxy centre (Figure 2). The averaged stellar rotation curve and velocity dispersion distribution are shown in Figure 3. The following orientation parameters were accepted: the line-of-nodes position angle  $PA_{CG} = 150 \pm 5$  deg, the inclination  $i_{CG} = 49 \pm 10$  deg. These values, based on the analysis of the SDSS  $r$ -band image slightly differ from the values calculated in Brosch et al. (2010) from the stellar kinematics ( $127 \pm 4$  and  $50 \pm 15$  deg, respectively). We think that the morphological  $PA_{CG}$  is more reliable in comparison with the kinematic one due to the large scatter of stellar velocities presented along both slit positions in (Brosch et al. 2010).

For the external ring we have accepted the  $PA_{ring} = 49 \pm 3$  deg, and the inclination of  $i_{ring} = 50 \pm 10^\circ$  according to Brosch et al. (2010) estimation from the circular model fitting of the ionized-gas velocity field. The corresponding H $\beta$  velocity field is shown in (Figure 4), the inner part was masked because of a strong contamination from the stellar absorption (see Fig. 7 in Brosch et al. 2010), the rotation curve is presented in Figure 3.

The present combination of  $(PA_{ring}, i_{ring})$  and  $(PA_{CG}, i_{CG})$  provides two solutions (eq. (1) in Moiseev 2008) for the mutual angle between the central galaxy and polar ring (denoted as  $\delta$  on the Fig. 1):  $73 \pm 12^\circ$  and  $58 \pm 9^\circ$ .

**Table 1.** Log of the observations

Galaxy	Slit PA (deg)	Date	Slit width (arcsec)	Sp. range (Å)	Sp. resol. (Å)	Exp. time (min)	Seeing (arcsec)
SPRC-7	150	5 Apr 2011	1.0	3900–5700	5.0	120	1.5
NGC 4262	0	3 Apr 2013	0.7	3700–7240	3.7	140	3.1
	160	6 Apr 2013	0.5	3700–7240	3.0	100	3.0

**Figure 2.** The results of the SAO RAS 6-m telescope long-slit observations: line-of-sight velocities and velocity dispersion of stars along the major axis. The dotted lines mark the position of nucleus and accepted systemic velocity.**Figure 3.** The observed rotation curves of the stars and gas components and mean line-of-sight velocity dispersion radial distribution in SPRC 7 (left) and NGC 4262 (right). The ‘high’ and ‘low’ data points correspond to the H I data with  $66 \times 17$  and  $79 \times 30$  arcsec beam size.

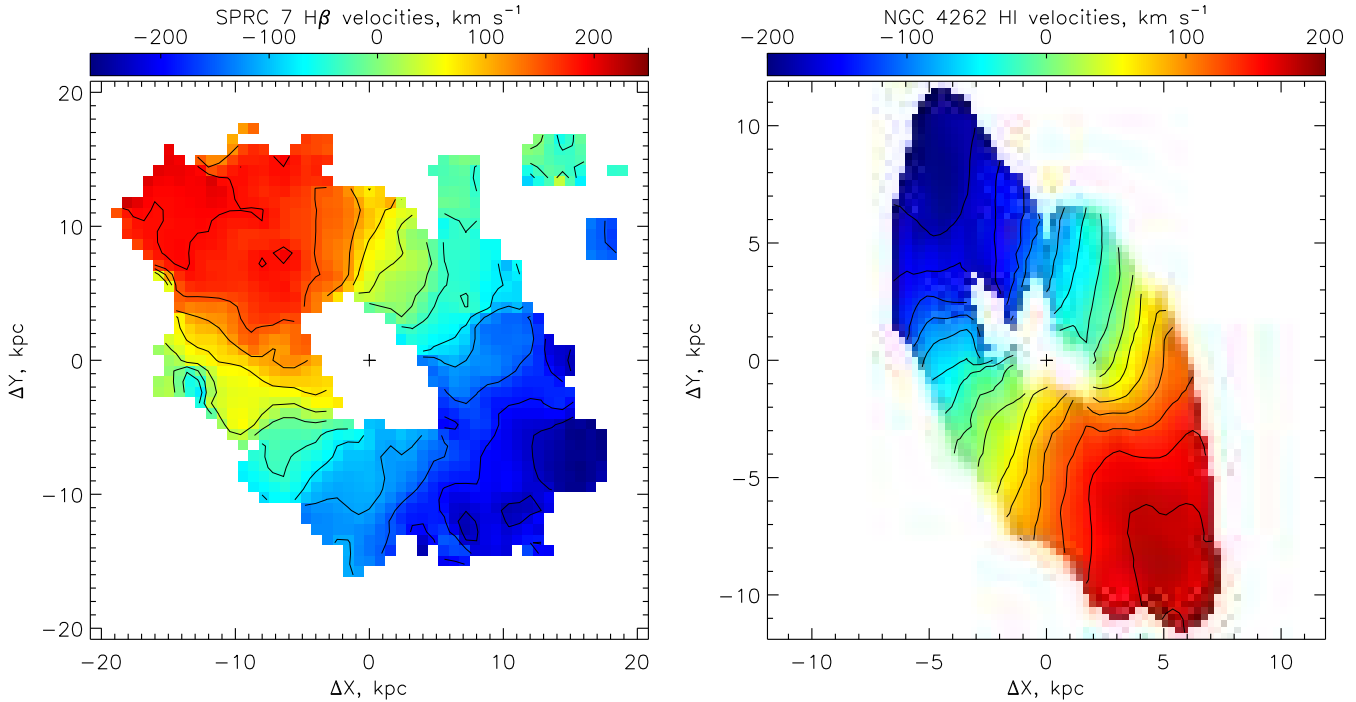


**Figure 4.** The line-of-sight velocity fields of the polar components ( $V$ ), after subtracting the systemic velocities: for the ionized gas in SPRC 7 (left) and for the H I in NGC 4262 (right). The cross marks the rotation centre position. North is upwards, east is to the left.

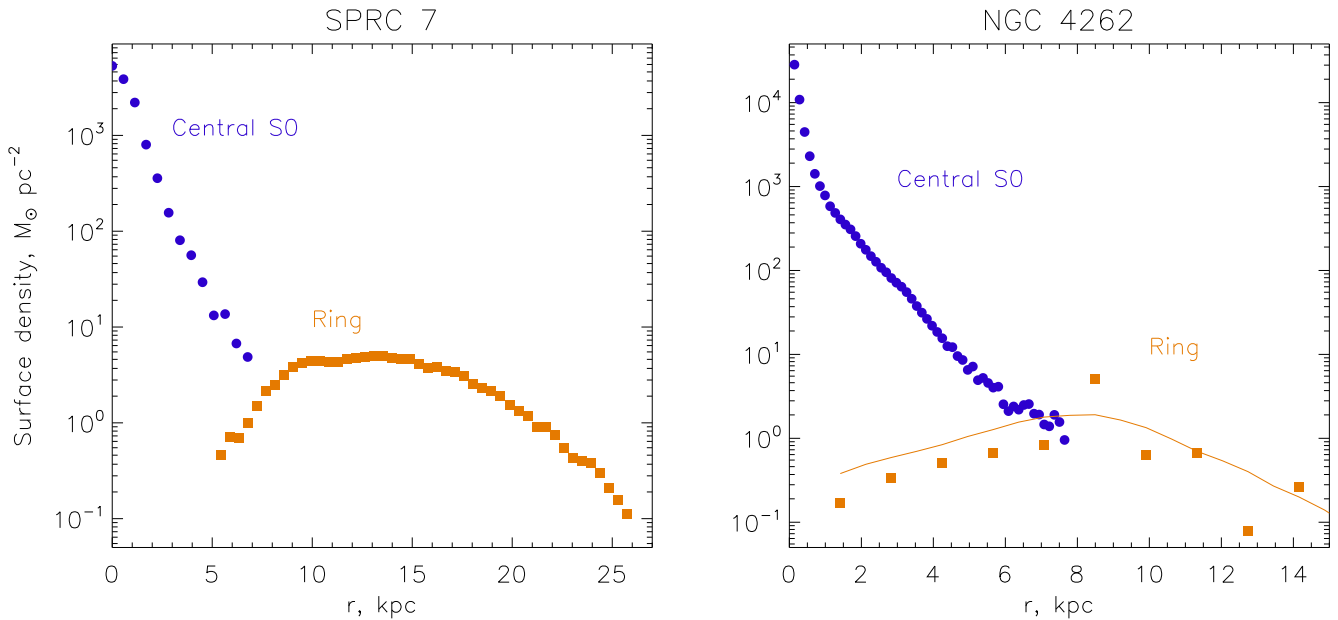


**Figure 5.** The azimuthally averaged mass density distribution for the internal and external components. In the case of SPRC 7 (left) both curves correspond to the mass density of stars derived from the SDSS data (see the text). In the NGC 4262 (right) the stellar mass was estimated only for the central galaxy. For the ring the figure shows the surface density of the gas ( $1.4 \times M_{\text{HI}}$ ) derived from the TiRiFiC model (orange symbols) and an azimuthally averaged density map (the orange curve).

We accepted the first value as a more stable case (i.e. the closest to the polar plane).

The surface density distributions of the stellar mass were calculated separately for each component using the  $g$  and  $r$  SDSS DR8 images averaged in the ellipses with the

corresponding  $PA$  and  $i$  (see Fig. 5). We use the foreground Galactic extinction values from the NED<sup>1</sup> and K-corrections

<sup>1</sup> <http://ned.ipac.caltech.edu>

from Chilingarian et al. (2010). The mass-to-luminosity ratios ( $M/L$ ) were calculated in each radii using  $(g-r)$  color according to Bell et al. (2003). The CG has a negative gradient of  $r$ -band  $M/L$  from  $\sim 7$  in the nucleus to 2 at the periphery. While in the blue ring this value is constant of the order of  $0.5 M_{\odot}/L_{\odot}$ .

### 2.3 NGC 4262

NGC 4262 is a well-known lenticular barred galaxy in the Virgo cluster, the accepted distance is 14.6 Mpc according to the *HST* photometry (Jordán et al. 2005) that corresponds to the scale of 0.071 kpc per arcsec. In contrast to the previous case, the polar component in NGC 4262 has no significant stellar mass contribution, while the galaxy is surrounded by an extended gaseous ring discovered in the 21 cm radio data by Krumm, van Driel & van Woerden (1985). Bettoni, Buson & Galletta (2010) have shown that: (i) the UV *GALEX* images reveal the presence of a young stellar population in the ring of neutral hydrogen; (ii) both the ionized gas in the inner region and the neutral hydrogen at large distances from the centre rotate in the plane, which is strongly inclined to the stellar disc of the galaxy. The contamination of UV knots in the optical SDSS images is very faint. Hence, in our simulations we have accepted a pure gaseous disc for this galaxy. Bettoni et al. (2010) prefer to speak of an inclined ring, but a formal calculation of the mutual inclination angle yields two solutions: 39 and 90 deg. The latter corresponds to the polar ring, as noted in their subsequent work (Buson, Bettoni & Galletta 2011).

We have observed the stellar kinematics of NGC 4262 in two slit positions, corresponding to two possible orientations of the CG line-of-nodes. The first one is  $PA = 160^{\circ}$ , what corresponds to the prolonged ‘plateau’ in the radial profiles of ellipticity and  $PA$  of the SDSS isophotes (see Figure 4 in Bettoni et al. 2010). However, external isophotes turn to the value of  $PA = 0^{\circ}$  (i.e.  $180^{\circ}$ ) together with a decrease of their ellipticity. The stellar velocity field of the central region was taken with SAURON integral field spectrograph (Emsellem et al. 2004). Our analysis of this velocity field in the framework of pure circular rotation approximation (‘tilted-rings’) also gives the kinematical  $PA \approx 0^{\circ}$  for the central region ( $r < 25''$  i.e. 1.8 kpc). However, the strong stellar bar can distort the velocity field on the scales of  $r \leq 1.5$  kpc from the centre. Using the long-slit data we took the stellar kinematics measurements up to  $\sim 4$  kpc from the nucleus. Two conclusions were obtained: (i) velocity distributions along both  $PA$ s have the best agreement between each other for  $PA_{CG} \approx 160^{\circ}$ ; (ii) the South half of the radial velocity curve shows an unusual decrease of the rotation curve in the external region (Figure 2). We suspect that this distortion may be related to the warping of this part of the stellar disc, or perhaps to the contamination from the ring material, because the projected gas velocities in this part of the ring (see the velocity field in Figure 4) are also redshifted relative to the systemic velocity.

These peculiar velocity points were excluded from the calculation of the final averaged stellar rotation curve shown in Figure 3. The accepted orientation parameters are  $PA_{CG} = 160 \pm 10^{\circ}$  and  $i_{CG} = 36 \pm 4^{\circ}$ . The last value was obtained from our approximation of the isophote ellipticity at  $r = 40 - 55$  arcsec from Bettoni et al. (2010) profiles.

For the analysis of the ring kinematics we used the results of the 21 cm WSRT radio observations presented by Oosterloo et al. (2010). Two H I data cubes denoted below as ‘high’ and ‘low’ with the angular resolution (beam) of  $66 \times 17$  and  $79 \times 30$  arcsec, respectively, were involved in the study. The H I velocity field for the high-resolution case is shown in the Figure 4. In order to take into account a strong elongation of the beam shape we used the TiRiFiC software<sup>2</sup>, specially designed for the H I data cubes fitting (Józsa et al. 2007).

Before modeling we masked the regions of the data cubes where strong noncircular motions occur. These regions are associated with active star formation visible in the *GALEX* image of NGC4262. During the modeling we have assumed that the position angle and inclination are constant with radius, whereas the H I surface density and rotation velocity vary with galactocentric distance. We have also considered a model, where the inclination and position angle could vary with radius, representing a warp. However in this model we did not obtain a significant warp. The position angle and inclination were different from that found for the flat disc model only for the inner part of the disc where the evaluations were not firm due to the low density of H I. Furthermore, the warped model did not reproduce the data cube better than the flat disc one. Hence, we chose the model with the constant position angle and inclination.

The obtained orientation parameters, as well as the rotation velocities show a good agreement for the high- and low-resolution data (see the rotation curve in Figure 3). For the accepted  $PA_{ring} = 215 \pm 2^{\circ}$ ,  $i_{ring} = 65 \pm 3^{\circ}$  the mutual angle between CG and ring is  $\delta = 50 \pm 6^{\circ}$  and  $\delta = 88 \pm 6^{\circ}$ . The last value corresponds to the true polar orientation.

The radial distribution of stellar surface density for the CG was calculated in a similar way with SPRC-7. The derived  $M/L$  values show a negative gradient from 4.5 in the centre up to  $1.5 M_{\odot}/L_{\odot}$  at the periphery. For the gaseous ring surface density distribution we used an azimuthally averaged profile derived from the H I density map. This profile has a smoother shape compared with the TiRiFiC results (see Figure 5) because some high-density regions were excluded from the model fitting (see above).

## 3 MODELLING, DECOMPOSITION AND FITTING

### 3.1 Modelling and decomposition

Full set of observational data let us to use standard assumption of the asymmetric drift for simulation of central galaxy rotation curve  $V_*$ , in the following form:

$$V_*^2 = \left(V_c^{obs}\right)^2 + \sigma_r^2 \left[ 1 - \frac{\sigma_{\varphi}^2}{\sigma_r^2} + \frac{r}{\rho\sigma_r^2} \frac{\partial(\rho\sigma_r^2)}{\partial r} + \frac{r}{\sigma_r^2} \frac{\partial\langle uw \rangle}{\partial z} \right], \quad (1)$$

where  $\frac{r}{\sigma_r^2} \frac{\partial\langle uw \rangle}{\partial z}$  is the chaotic part of the radial  $u$  and vertical  $w$  velocity components and this term usually equals zero. This stability criterion assumes the radial equilibrium of the disc towards the gravitational instability.

<sup>2</sup> <http://www.astron.nl/~jozsa/tirific/>

**Table 2.** Parameters of PRGs from the photometric data.

Name	$D$ Mpc	$i_{ring}$ °	$i_{CG}$ °	$\delta$ °	$r_d$ $10^{10} M_\odot$	$M_b$ kpc	$r_b$ $10^{10} M_\odot$	$r_b^{max}$ kpc	$M_1$ kpc	$R_{disc}$ kpc	$R_{PR}$ kpc
SPRC 7	261.6	$50 \pm 10$	$49 \pm 10$	$58 \pm 9 / 73 \pm 12$	1.77	0.97	3.4	0.8	4	3.7	23
NGC 4262	14.6	$65 \pm 3$	$36 \pm 4$	$50 \pm 6 / 88 \pm 6$	1.02	0.9	0.4	0.2	1	4.2	15

$D$  — distance;  $i_{ring}$  — inclination angle of the central galaxy;  $i_{CG}$  — inclination angle of the polar component;  $\delta$  — relative angle between CG and polar component;  $r_d$  — radial exponential scale length of the central disc;  $M_b$  — bulge mass;  $r_b$  — bulge scale;  $r_b^{max}$  — bulge size;  $M_1$  — polar ring mass;  $R_{disc}$  — outer radius of the CG;  $R_{PR}$  — outer radius of the polar ring.

An important issue here is the determination of velocity dispersion profiles from the observed ones. Radial velocity dispersion can be obtained from the measured dispersion along the major axis  $\sigma_{obs}$ :

$$\sigma_r = \sigma_{obs} \cdot [(\sigma_\varphi/\sigma_r)^2 \sin^2 i_{CG} + (\sigma_z/\sigma_r)^2 \cos^2 i_{CG}]. \quad (2)$$

The first part of the right side of this equation is determined by the Lindblad formula for the epicyclic approximation  $\sigma_\varphi/\sigma_r = \kappa/2\Omega$ , where  $\kappa$  is the epicyclic frequency and  $\Omega \equiv V_*/r$ . In general, for disc galaxies the ratio  $\sigma_z/\sigma_r$  lies in the interval of 0.5 – 0.8 (Shapiro, Gerssen & van der Marel 2003; van der Kruit & Freeman 2011). However, the detailed simulations of individual early-type galaxies with the dynamically hot discs, which are similar to our galaxy sample provide larger values up to  $\sigma_z/\sigma_r \approx 1$  (Zasov et al. 2012). Dynamical models of the individual galaxies demonstrate the variation of the  $\sigma_z/\sigma_r$  ratio along the galactic radius and this relation depends on the parameters of the galaxy (Khoperskov et al. 2010; Zasov et al. 2012). However, here in the simulations we neglect this effect. In this work we have used the ratio 0.9 for both galaxies. Fortunately, this choice does not critically affect our results. As a demonstration, we show in Figure 6 the circular velocities reconstructed for both galaxies with different values of  $\sigma_z/\sigma_r$ . It is clearly seen that the uncertainties are within the 5 – 10% scatter from the mean value. Previous assumptions give us a possibility to reconstruct the circular velocity of stars, which corresponds to the observational galactic rotation velocity  $V_c^{obs}$ .

Circular velocity of the central disc or rotation velocity of the gaseous polar component unambiguously determines the total gravitational potential of the system:

$$-V_c(r_1)^2 = -r_1 \frac{\partial \Psi_{tot}}{\partial r_1}, \quad (3)$$

$$-V_g(r_2)^2 = -r_2 \frac{\partial \Psi_{tot}}{\partial r_2}, \quad (4)$$

where  $r_1 = \sqrt{x^2 + y^2}$  and  $r_2 = \sqrt{x^2 + (z \sin(\delta))^2}$ . The total gravitational potential is the superposition of the stellar disc, bulge, polar ring and dark matter halo potentials:

$$\Psi_{tot} = \Psi_{disc} + \Psi_{bulge} + \Psi_{ring} + \Psi_{halo}. \quad (5)$$

We have used the exponential disc  $\Psi_{disc}$  and King’s bulge approximation  $\Psi_{bulge}$  with the parameters given in table 2. The following model was used for the polar ring contribution to the total gravity:

$$\Psi_{ring}(r) = -\frac{GM(<r)}{r}. \quad (6)$$

It is believed that the mass of the polar ring should be rather small and it is not sufficient to greatly affect the total grav-

ity. However, for the SPRC 7 the estimated mass is  $10^8 M_\odot$ , which gives the circular velocity of up to  $50 \text{ km s}^{-1}$ . In contrast, the gaseous mass of NGC 4262 is four times smaller and its own circular velocity does not exceed  $25 \text{ km s}^{-1}$ .

To reproduce the observed rotation velocity, we need to constrain the parameters of the dark matter halo potential. Two profiles of matter distribution in the halo were used for this purpose: NFW model (Navarro, Frenk & White 1997) and isothermal halo model (Burkert 1995). As it was mentioned above, copious previous research has revealed that the halo is not spherical. So, the most general case is that the halo is an ellipsoid, and its scale length also depends on the coordinates. Following Hayashi, Navarro & Springel (2007) we modify the standard potential profiles this way:

$$\Psi_{halo}(x, y, z) = \Psi_{halo}(\xi), \quad (7)$$

where

$$\xi = r \sqrt{\left[\frac{x}{a_h(r)}\right]^2 + \left[\frac{y}{b_h(r)}\right]^2 + \left[\frac{z}{c_h(r)}\right]^2}. \quad (8)$$

with normalization  $r^3 = a_h(r)b_h(r)c_h(r)$  and  $a_h(r) = r(b/a)^{-1/3}(c/a)^{-1/3}$ . The kinematics of polar ring galaxies allow to directly constrain the halo parameters for two axes: in the disc plane  $a_h$  and in the perpendicular direction  $c_h$ , which is equivalent to the pair of parameters  $a_h$  and  $c/a$  where  $a_h$  does not depend on radius  $r$ . Below we assume that the third halo’s scale length  $b_h$  is equal to  $a_h$ .

In the next paragraph, we describe the models of the halo potential and the fitting methods for the kinematics of PRGs.

### 3.2 Fitting procedure

We can indicate three types of haloes from the previous part:

- Spherical halo, if  $a_h = c_h$ . There are two parameters: the mass of the halo  $M_h$  and its scale length.
- Oblate halo, if  $a_h \neq c_h$  and we have three free parameters:  $M_h$ ,  $a_h$  and  $c/a$ .
- Variable shape halo,  $c/a$  is a function of radius.

The last type requires a model of the halo axis variation. We use the following approximation obtained for the sample of simulated haloes within the  $\Lambda$ CDM framework (Hayashi et al. 2007):

$$c/a = \exp[\alpha \tanh(\gamma \log(r/r_\alpha))], \quad (9)$$

where the  $\alpha$ ,  $\gamma$  and  $r_\alpha$  parameters determine the character of the halo shape. These parameters are quite different for the potential and density distributions of the haloes, but the type of the shape variation is similar. It should be noted

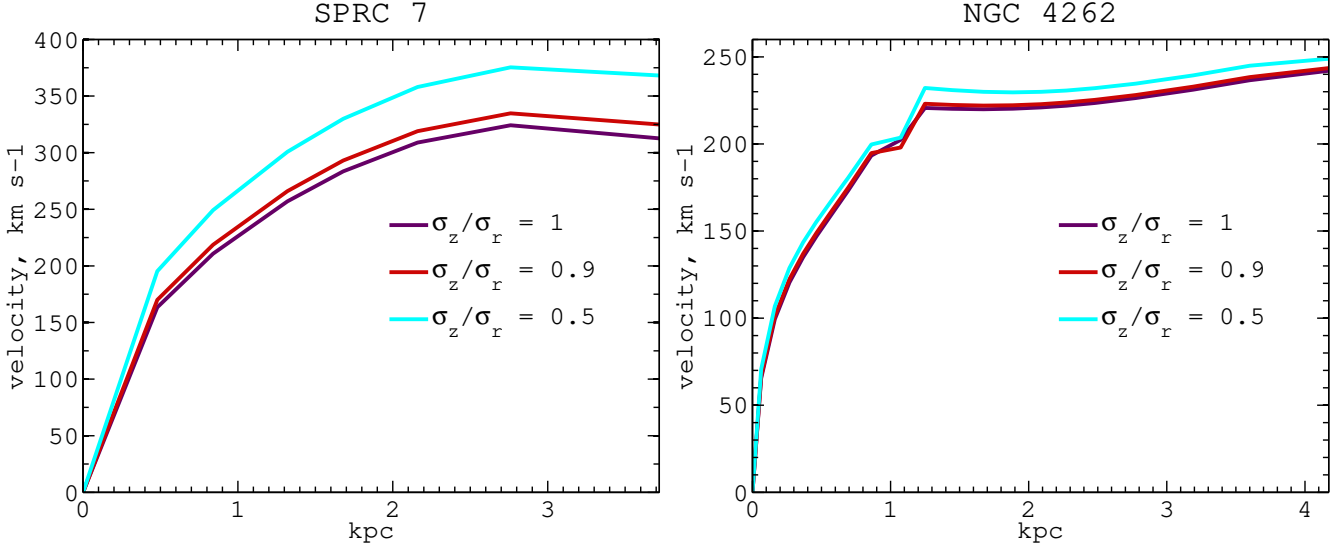


**Figure 6.** The circular velocities  $V_c^{obs}$  for SPRC 7 (left) and NGC 4262 (right) reconstructed from equation (3.1) with different values of  $\sigma_z/\sigma_r$ .

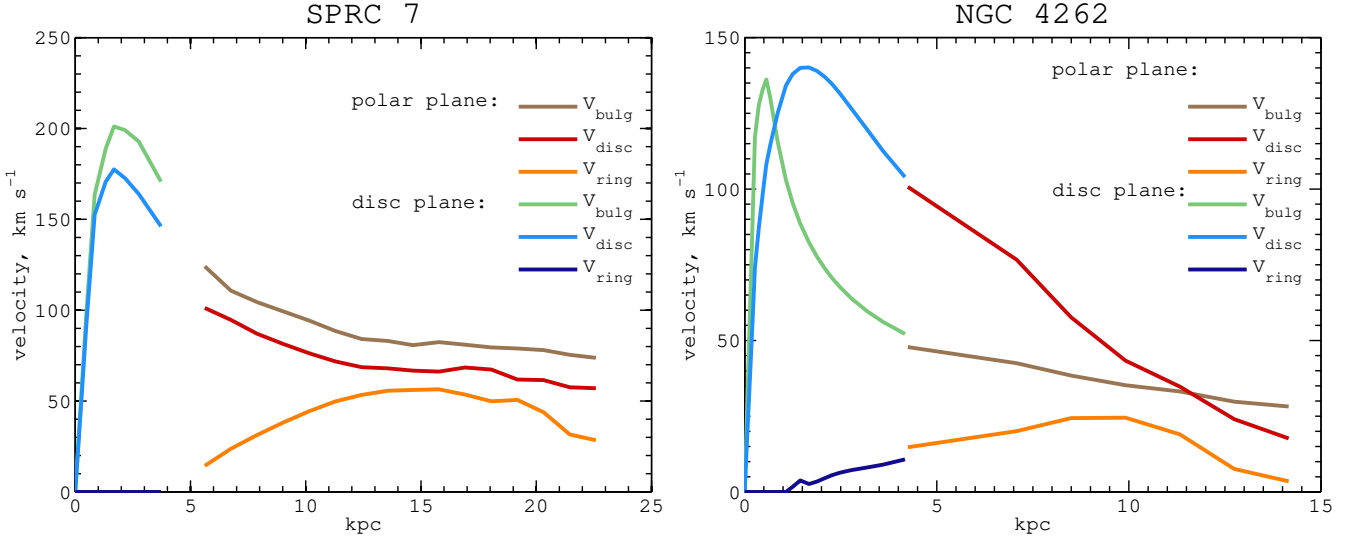


**Figure 7.** The components of circular velocities for the bulge, the disc and the ring in SPRC 7 (left) and NGC 4262 (right).

that the formula describes well both the density and potential distribution of DM in the halo. Formally, such a model gives five free parameters:  $M_h$ ,  $a_h$ ,  $\alpha$  parametrizes the central value of the halo axis ratio and it is given by  $10^{-2\alpha}$ ,  $r_\alpha$  is the characteristic radius at which the axial ratio increases significantly from its central value and  $\gamma$  regulates the sharpness of the halo shape.

We examine the different types of dark matter potential which can reproduce both the observed kinematics of the gaseous polar ring and the stellar kinematics in the central galaxy simultaneously. Thus, our aim is to find the halo parameters producing the minimal differences:

$$(V_c - V_c^{obs})^2 / (\delta V_c^{obs})^2 = \chi_s^2, \quad (10)$$

$$(V_g - V_{gas})^2 / (\delta V_{gas})^2 = \chi_g^2, \quad (11)$$

where  $V_c$  and  $V_g$  are given by (3) and (4) correspondingly, and  $\delta V_c^{obs}$ ,  $\delta V_{gas}$  are the observational uncertainties of the velocities. However, a more flexible approach is to minimize the normalized superposition of  $\chi_s^2$  and  $\chi_g^2$ :

$$\chi^2 = \chi_s^2/n_s + \chi_g^2/n_g, \quad (12)$$

where  $n_s$  and  $n_g$  are the numbers of observational points on the rotational curves.

In order to fix some systematic features of the kinematics of the polar gaseous components (an elongated beam for NGC 4262, a possible spiral structure in SPRC 7) we do not fit the whole velocity fields. To convert the data from the simulated gas velocity field to the one-dimensional rotation curve, we have used a simple assumption of quasi-circular motion in the ring (see Moiseev & Mustsevoi 2000, and references therein). In the polar coordinates in the sky plane

there is a relation between the line-of-sight velocity field  $V(r, PA)$  and the de-projected rotation curve of gas:

$$V(r_2, PA) = V_g(r_2) \frac{\cos(PA - PA_0)}{(1 + \sin^2(PA - PA_0) \tan^2 i_1)^{1/2}}, \quad (13)$$

where  $r$  is the distance from the rotation center,  $PA$  is the position angle in the sky plane and  $PA_0$  is the line-of-nodes position angle. The rotation curve was calculated through the minimization of the difference between the left and right sides of the equation (13).

To take into account the azimuthal inhomogeneity of the velocity field caused by the perturbation from the central galaxy and from the non-spherical DM halo, we have simulated the velocity field in ballistic assumption. After that we obtain  $V_g$  using equation (13). Thus, we have the gaseous rotation curves from the observations, and the simulated velocity fields as well.

The fitting procedure is accomplished using a combination of simulated annealing and downhill simplex methods. On every single step of the fitting we vary the parameters of the DM halo and hence circular velocities change too.

## 4 RESULTS

### 4.1 SPRC-7

The simulations of the kinematics of this galaxy allow us to conclude that the models of spherical halo can not accurately reproduce the rotation of both components of SPRC 7. It is clearly seen that these best-fit models produce a smaller circular velocity of CG and faster rotation of the polar component than those expected from the observations (see Figure 8). This discrepancy is especially well seen in a comparison of rotation curves of CG and models. The spherical halo model does not reproduce the flat part of the rotation curve at  $r = 2-4$  kpc, where the difference is about  $50-70$  km s<sup>-1</sup>. This result is not surprising, because it agrees with numerous previous investigations of PRGs. We found that best-fit model of the potential for SPRC 7 is the halo flattened towards the polar plane with the axis ratio  $c/a = 1.7 \pm 0.2$  for the isothermal halo model and  $c/a = 1.5 \pm 0.2$  for NFW. Figure 8 shows both of these models. The masses of haloes are also quite close to each other:  $1.5 \pm 0.2 \cdot 10^{11} M_\odot$ , for the isothermal halo and  $1.9 \pm 0.1 \cdot 10^{11} M_\odot$  for the NFW halo profile. Basically, the deviation of the model rotation curve from the observations is not high for all types of models (flattened or spherical halo) shown here. The general difference is in the central part of the polar ring, where the residual velocity is about  $40-50$  km s<sup>-1</sup>. However, even such values are within the error bars. The distinctive feature of various solutions is in the kinematics of CG. Large values of circular velocity (e.g. Figure 6) up to  $300$  km s<sup>-1</sup> require a relatively short halo axis in the CG plane. At the same time, a slow growth of the rotation curve with radius is provided by the large halo axis in the polar plane. The combination of both of these aspects gives us a flattened halo towards the polar plane.

### 4.2 NGC 4262

The variation of the halo mass  $M_h$ , halo scale length  $a$  and halo axis ratio  $c/a$  didn't bring a sufficient result for the

reconstructed disc and ring rotation. It is well seen in the Figure 9 that the model curves have a bad agreement with the observations, especially for the rotation curve of the polar ring for the models with  $c/a = 1$  and  $c/a = const$ . The reason is as follows. It is obvious that circular velocity for the central galaxy is significantly higher than the measured rotation curve because of the asymmetric drift. The fact that the polar ring rotates in another plane than the host galaxy, the inner part should rotate with approximately the same velocity. For instance, the maximum value of circular velocity for NGC 4262 is  $240$  km s<sup>-1</sup> (Figure 6), but the inner edge of the ring rotates at  $160$  km s<sup>-1</sup> (figure 3). Moreover, in this region the ring rotates slower than the central galaxy in contrast to the SPRC 7. Here we can summarize that a simple oblate/prolate or spherical DM halo shape does not explain the observations (see Figure 9).

To achieve a good agreement between the observations and model of PRG rotation, we propose a more complicated shape of DM halo following the cosmological numerical simulations (Hayashi et al. 2007). We study the possibility of the variable DM halo shape in the form (9) described in the previous Section. It should be noted that following the approximation, the simulated haloes are usually prolate. However, they become less axisymmetric and more spherical in the outer regions. It is not clear how to translate this result directly to our units, because Hayashi et al. (2007) did not consider the baryon fraction and there is no opportunity to estimate the arrangement of the galactic disc in their model haloes. Furthermore, the condensation of baryons should lead to rounder halos (Debattista et al. 2008). Nevertheless, we assume that a simple approximation of the halo shape is a common case.

We apply the fitting procedure for the kinematics of NGC 4262 accounting for the assumption of the variable shape of DM halo. This provides the 5-dimensional phase space of the parameters:  $M_h$ ,  $a_h$ ,  $\alpha$ ,  $\gamma$  and  $r_\alpha$ . The best-fit rotation for both components of the galaxy is shown in Figure 9. We have found that the DM halo is oblate within the optical radius of the central galaxy and at the same time the halo is strongly flattened towards the perpendicular (or polar) plane far beyond this radius. The corresponding halo axis ratio is shown in Figure 10. Both isothermal  $(c/a)_{iso}$  and NFW  $(c/a)_{NFW}$  models demonstrate similar profiles, but  $(c/a)_{NFW}$  has a much steeper slope. The central value is exactly the same and it is equal to  $0.4 \pm 0.1$ . The isothermal halo becomes round at  $r = 5.5-6$  kpc and NFW at  $r = 3-3.5$  kpc, these values are quite close to the optical size of CG. At the large radii, the halo axis ratio differs a bit:  $(c/a)_{NFW} = 2.3$  versus  $(c/a)_{iso} = 1.7$  at  $r = 15$  kpc. It is worth noting that large uncertainties exist especially at large distances from the galactic center. This is explained by the weak sensitivity of the model from the gravitational potential at the outer part of galaxy. The inner axis ratio is strictly smaller than unity, at the same time, despite the large error bars at the outer part halo axis ratio  $c/a$  is strictly larger than unity. Thus, we should underline that such kind of halo shape is strongly required to reproduce the observational kinematics of NGC 4262.

The quantitative discrepancy between the NFW- and isothermal DM shapes, shown in Figure 10 might be explained in the following way. We have fit the same kinematics by both the NFW and isothermal halo models having

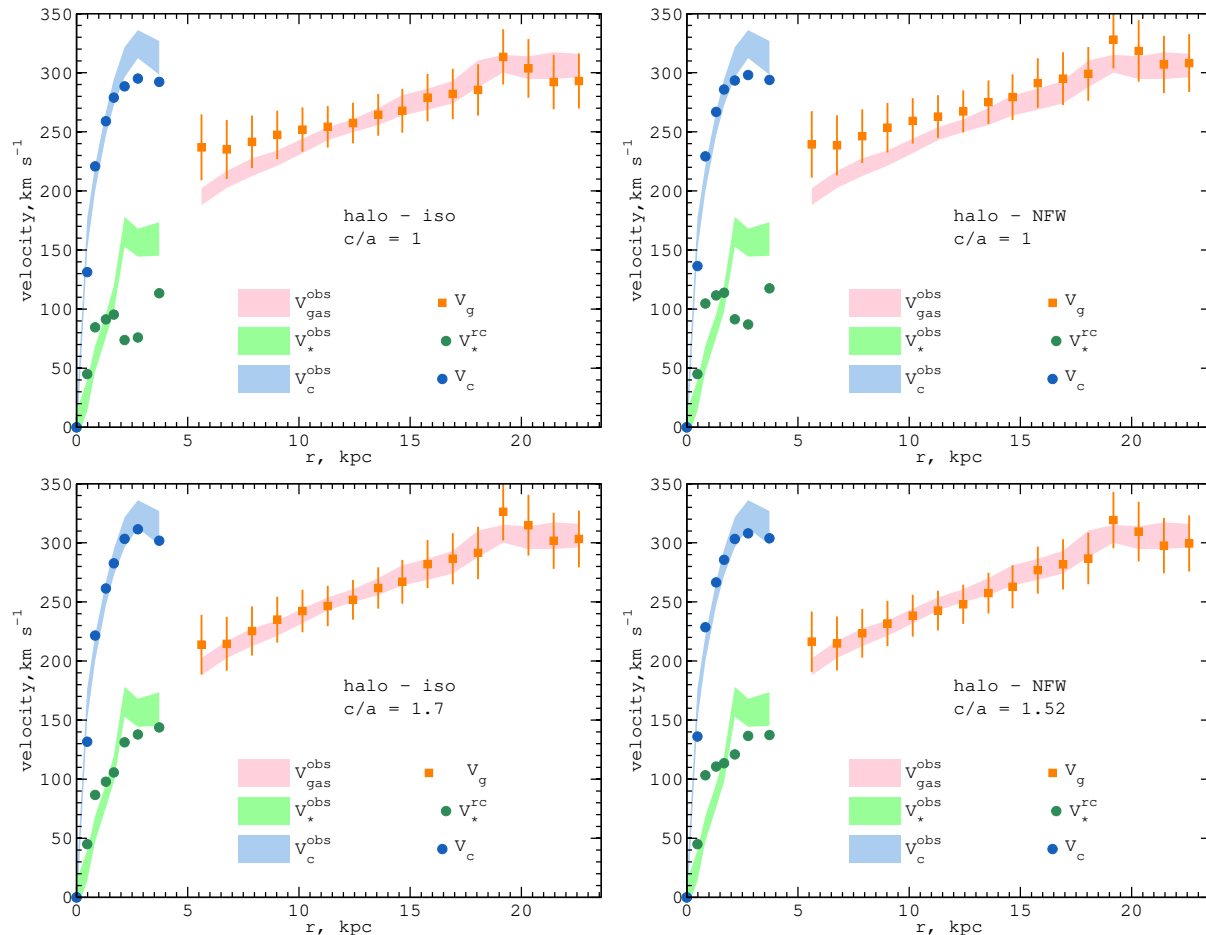


**Figure 8.** Left column: the best-fit models of rotation velocity for both components of SPRC 7 for the isothermal halo profile. Right column: the same, but for the NFW model. The first row corresponds to the spherical model ( $c/a = 1$ ). The second row is for the model with the constant  $c/a \neq 1$  ratio.

slightly different masses (Table 3). It is possible only in case of various halo axis ratio. Namely, a relatively larger halo mass explains the given galaxy kinematics in case of a larger deviation of the DM from the spherical shape. In Figure 10 NFW best fit model have larger values of  $c/a$ . Meanwhile, we can see from Table 3 that the mass of the DM halo with the NFW profile is systematically larger than in the isothermal profile for all models. This relation is in agreement with the cosmological simulations by (Allgood et al. 2006), where the major-to-minor axis ratio (always less than 1) decreases with the growing virial mass of the DM halo.

In this context, there comes a question about the possibility of separation of the NFW and isothermal profiles for the given galaxies if there exist both constrains on mass and the halo axis ratio. However, our solutions always overlap beyond the galactic center due to large uncertainties. Hopefully, a larger sample of DM shapes will yield more reliable conclusions.

## 5 DISCUSSION

We have investigated two polar ring galaxies in the context of the shape of the dark matter halo around them. We found the first estimates of the halo axis ratio for

SPRC 7 and NGC 4262. An expectable result for SPRC 7 is a halo flattened towards the polar ring plane. NGC 4262 becomes a more interesting case: it was shown that the halo axis ratio varies with radius from being flattened towards the CG plane in the center and up to being prolate towards the polar plane far beyond the CG. There are a few evidences that DM haloes have such kind of shape in our Galaxy. Banerjee & Jog (2011) justify the non-constant Milky Way halo axis ratios using the flaring of the H I layer. Meanwhile, evidences of varying halo axis ratio were found from the study of the Sagittarius stream. Vera-Ciro & Helmi (2013) have found that our Galaxy dark halo is oblate with  $c/a = 0.9$  (within 10 kpc) while the outer halo can be made mildly triaxial. It is possible that in general, the DM halo shape of the NGC 4262 is similar to the variable shape of the Galaxy.

Nevertheless, NGC 4262 is the first example of DM variable shape in a distant galaxy. Can it be proposed hypothesized in this context that an oblate central part and a prolate outer region is a common situation for the overwhelming amount of galaxies? It is not obvious now due to the poor sample of objects with well-measured dark matter halo properties. At the same time, the quality of the observational data for distant galaxies is slightly limited. Note

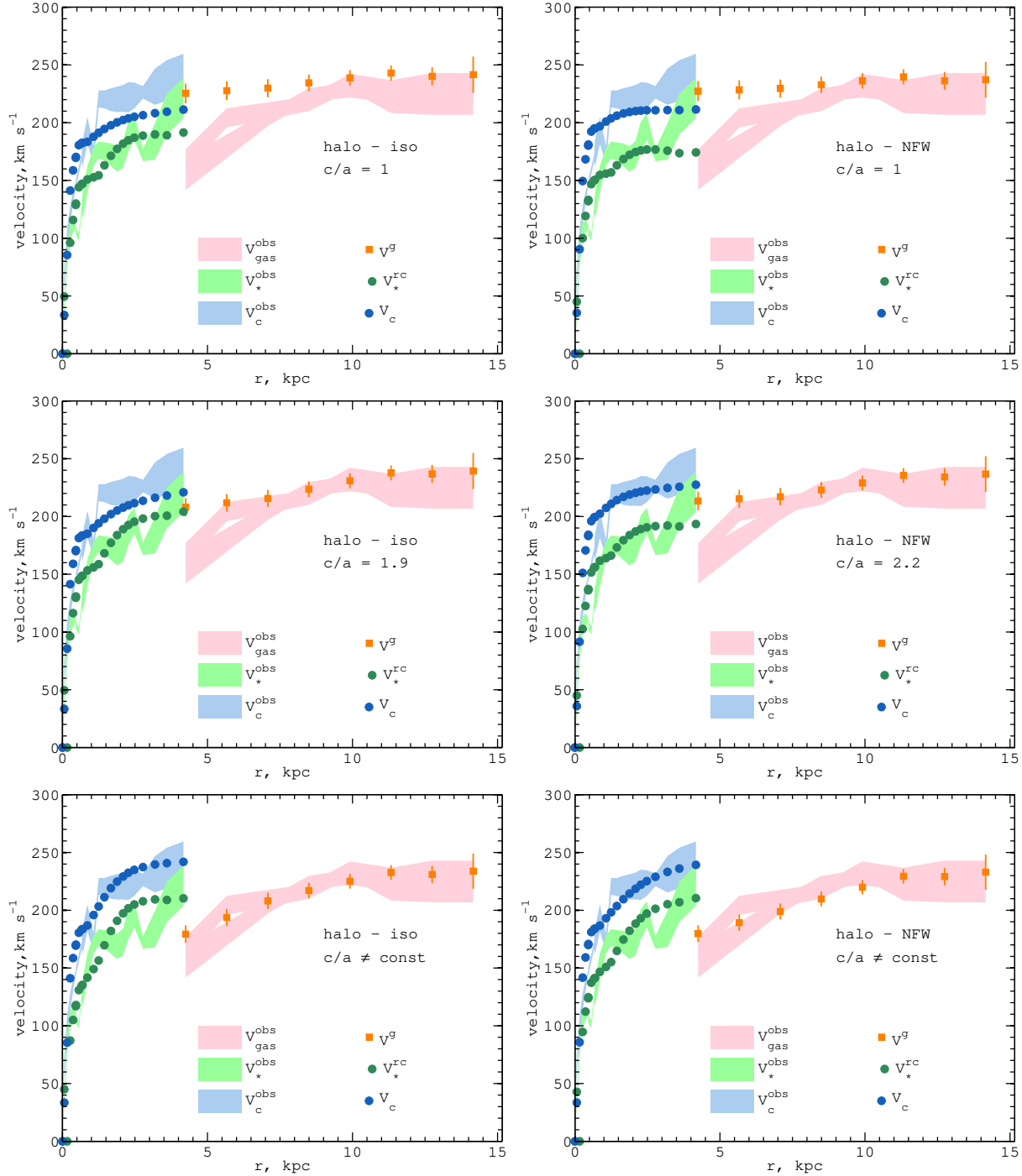


**Figure 9.** The same as in fig 8 but for NGC 4262. The third row is for the models with a variable halo axis ratio.

that NGC 4262 belongs to the Virgo cluster, and therefore, a strong interaction should have occurred during the galaxy formation history.

Both galaxies considered have large velocity dispersion inside the optical radius. Perhaps the main reason for this feature is related to the history of formation and evolution of galaxies, which is reflected in the dynamical overheating of the CG stellar component. It is likely that an external processes (gas accretion and/or tidal effects and/or mergers) are responsible for it.

Why are the resulting shapes of DM haloes for PRGs in our study different? On the one hand, both central galaxies have similar sizes and rotation curves with a large velocity dispersion going up to 200-250 km s<sup>-1</sup> in the center. A rather large amount of DM is needed to stabilize the dynamics of host galaxies.

However, a striking difference between these PRGs is the ring rotation character. It is clearly seen that the rotation velocity of the ring of SPRC-7 grows from 200 km s<sup>-1</sup> up to 320 km s<sup>-1</sup> and becomes larger than the circular velocity

**Table 3.** Best-fit halo parameters for the considered galaxies

Name (halo) model	$M_h$ ( $\leq 14$ kpc) $10^{11} M_\odot$	$a_h$ kpc	$c/a$	$\alpha$	$r_\alpha$ kpc	$\gamma$
SPRC 7 (iso) I	$1.81 \pm 0.52$	$1.82 \pm 0.5$	1	–	–	–
SPRC 7 (iso) II	$1.56 \pm 0.23$	$1.45 \pm 0.41$	$1.7 \pm 0.22$	–	–	–
SPRC 7 (NFW) I	$1.83 \pm 0.11$	$17.4 \pm 1.77$	1	–	–	–
SPRC 7 (NFW) II	$1.9 \pm 0.11$	$14.6 \pm 1.64$	$1.52 \pm 0.16$	–	–	–
NGC 4262 (iso) I	$1.25 \pm 0.16$	$1.7 \pm 0.48$	1	–	–	–
NGC 4262 (iso) II	$1.2 \pm 0.2$	$2 \pm 0.3$	$1.9 \pm 0.25$	–	–	–
NGC 4262 (iso) III	$1.6 \pm 0.2$	$2.4 \pm 0.46$	–	$0.9 \pm 0.3$	$1.33 \pm 0.2$	$0.68 \pm 0.09$
NGC 4262 (NFW) I	$1.5 \pm 0.15$	$14.8 \pm 2.7$	1	–	–	–
NGC 4262 (NFW) II	$1.8 \pm 0.3$	$13 \pm 2.1$	$2.2 \pm 0.7$	–	–	–
NGC 4262 (NFW) III	$1.9 \pm 0.4$	$11 \pm 2$	–	$0.93 \pm 0.3$	$0.95 \pm 0.1$	$1.1 \pm 0.2$

$M_h$  — halo mass within 14 kpcs;  $a_h$  — halo scale length along the X-axis in the host galaxy plane;  $c/a$  — halo axis ratio in polar and disc planes for the non-spherical halo model;  $\alpha$ ,  $r_\alpha$ ,  $\gamma$  — halo shape parameters in case of a variable axis ratio (see eq.9).

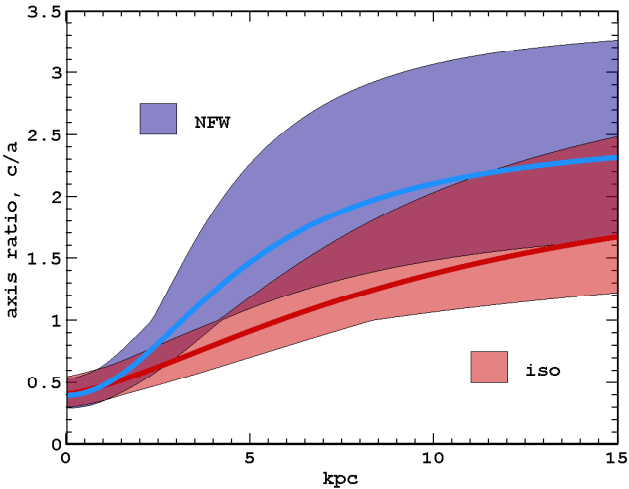


**Figure 10.** The axial ratios of DM halo of NGC 4262 as a function of radius in the best-fit models with radially varying shapes. The solid lines are the best-fit models of the halo axis ratio according to the parameters from the Table 3. The color regions mark the  $\pm 3\sigma$  range of the  $c/a$  ratio for the NFW halo model (blue) and the isothermal halo (red).

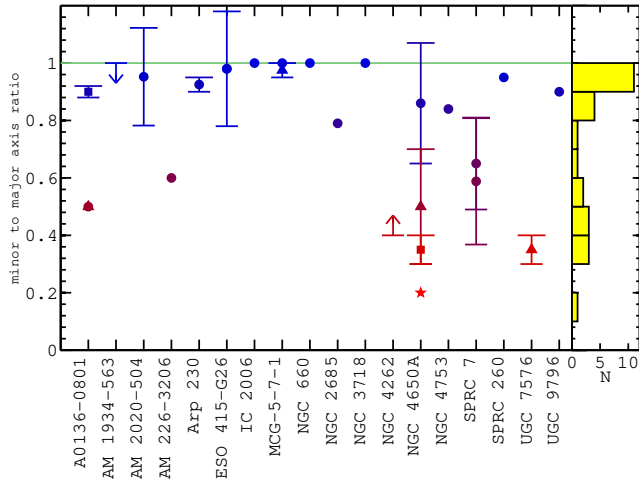
of the S0 disc. This rotation should be provided by the DM halo with a rather large scale length in the polar plane. This expectation is confirmed by our results. For NGC 4262 the situation is not as clear because the gaseous ring component rotates at a slower rate than the circular velocity of the S0 disc. The described pattern requires a more complicated shape of DM halo than the one obtained above. The previous research allowed us to analyze the halo axis ratio for 18 PRGs, including the current manuscript (see Figure 11). The halo shapes were estimated using various models along with diverse observational data (stellar and/or gaseous kinematics and/or photometrical data). Several galaxies have a few estimates for the halo shape, e.g. A0136-0801 — 3, MCG-5-7-1 — 2, NGC 4560A — 4 and SPRC 7 — 2 for different halo profiles. Generally, for the known sample of PRGs the shape of the halo is close to round  $c/a \approx 1$ . In the right panel of

Figure 11, the number of galaxies versus the minor-to-major axis ratio is shown by the yellow histogram. It is clearly seen that there is a bimodal distribution with the mean values of  $c/a \approx 1$  and  $c/a \approx 0.4$ . The recent statistics is certainly strongly limited. Nevertheless, the well-investigated galaxies (A0136-0801 and NGC 4560A) demonstrate scattered results which tend to  $c/a \approx 0.4$ . A possible explanation here is that most of the  $c/a$  estimates are the spatially averaged values, which are close to the round halo. As it was mentioned above, the expected shape of the DM halo should be more complex. However, the limitation arising from model assumptions and observational difficulties, which occurs due to the peculiar character of PRGs does not allow to carefully measure the halo shape for the majority of PRGs.

The fact that the polar component in many PRGs contains numerous H II regions indicates the ongoing large-scale star formation process. In massive rings, which are the gravitationally unstable tightly wound spiral structures can be developed (Theis et al. 2006). However, most of the rings are not massive enough for the gravitational instability, which might compress the gas up to the critical values. In this case, non-axisymmetric perturbations should play a decisive role. Effective perturbation sources are a massive central galaxy and a non-axisymmetric DM halo. Some authors were investigating the reaction of the gaseous disc to the presence of a non-spherical DM halo (Bekki & Freeman 2002; Masset & Bureau 2003; Khoperskov et al. 2012). These results should be directly projected to the polar ring galaxies.

## 6 ACKNOWLEDGEMENTS

The authors thank the anonymous referee for helpful comments. We would like to thank Tom Oosterloo, who has kindly provided the processed H I data cubes of NGC4262. We are grateful to Gyula Józsa for providing the TiRiFiC software and technical advise on its usage. This work was supported by the RFBR grants no. 12-02-31452, 13-02-00416 and by the “Active Processes in Galactic and Extragalactic Objects” basic research program of the Department of Physical Sciences of the RAS OFN-17. S.K., A.M., and A.S. are also grateful for the financial support of the ‘Dy-



**Figure 11.** The minor-to-major axis ratio of the DM halo obtained for different well-studied PRGs: A0136-0801 (Sackett et al. 1994; Sackett & Pogge 1995), AM 1934-563 (Brosch et al. 2007), AM 2020-504 (Arnaboldi et al. 1992), AM 226-3206 (Whitmore et al. 1987), Arp 230 (Schiminovich et al. 2013), ESO 415-G26 (Whitmore et al. 1987), IC 2006 (Franx, van Gorkom & de Zeeuw 1994), MCG-5-7-1 (Cox & Sparke 1996; Schiminovich et al. 2013), NGC 660 (van Driel et al. 1995), NGC 2685 (Peletier & Christodoulou 1993), NGC 3718 (Sparke et al. 2009), NGC 4262 (this work), NGC 4650A (Whitmore et al. 1987; Sackett & Sparke 1990; Sackett et al. 1994; Combes & Arnaboldi 1996), NGC 4753 (Steiman-Cameron, Kormendy & Durisen 1992), NGC 5122 (Cox & Sparke 1996), NGC 5907 (Reshetnikov & Sotnikova 2000), SPRC 7 (this work), SPRC 260 (Khoperskov, Moiseev & Khoperskov 2013), UGC 4261 (Reshetnikov, Hagen-Thorn & Yakovleva 1998), UGC 7576 (Sparke 2002), UGC 9796 (Cox, Sparke & van Moorsel 2006).

nasty' Foundation. The observations obtained with the 6-m telescope of the Special Astrophysical Observatory of the Russian Academy of Sciences were carried out with the financial support of the Ministry of Education and Science of Russian Federation (contracts no. 16.518.11.7073 and 14.518.11.7070). This research has made use of the NED database, which is operated by the Jet Propulsion Laboratory, California Institute of Technology, under the contract with the National Aeronautics and Space Administration. The funding for the SDSS has been provided by the Alfred P. Sloan Foundation, the Participating Institutions, the National Science Foundation, the United States Department of Energy, the National Aeronautics and Space Administration, the Japanese Monbukagakusho, the Max Planck Society and the Higher Education Funding Council for England.

**References**

Abadi M. G., Navarro J. F., Fardal M., Babul A., Steinmetz M., 2010, *MNRAS*, 407, 435  
 Afanasiev V. L., Moiseev A. V., 2005, *Astronomy Letters*, 31, 194  
 Afanasiev V. L., Moiseev A. V., 2011, *Baltic Astronomy*, 20, 363

Allgood B., Flores R. A., Primack J. R., Kravtsov A. V., Wechsler R. H., Faltenbacher A., Bullock J. S., 2006, *MNRAS*, 367, 1781  
 Arnaboldi M., Capaccioli M., Cappellaro E., Held E., Sparke L. S., Mackie G., 1992, in Dermott S. F., Hunter Jr. J. H., Wilson R. E., eds, *Astrophysical Disks Vol. 675 of Annals of the New York Academy of Sciences*, The polar ring galaxy AM 2020-504. pp 207–216  
 Athanassoula E., 2013, *ArXiv e-prints*  
 Athanassoula E., Machado R. E. G., Rodionov S. A., 2013, *MNRAS*, 429, 1949  
 Bailin J., Steinmetz M., 2005, *ApJ*, 627, 647  
 Banerjee A., Jog C. J., 2011, *ApJL*, 732, L8  
 Begeman K. G., Broeils A. H., Sanders R. H., 1991, *MNRAS*, 249, 523  
 Bekki K., Freeman K. C., 2002, *ApJL*, 574, L21  
 Bell E. F., McIntosh D. H., Katz N., Weinberg M. D., 2003, *ApJS*, 149, 289  
 Belokurov V., Koposov S. E., Evans N. W., Peñarrubia J., Irwin M. J., Smith M. C., Lewis G. F., Gieles M., Wilkinson M. I., Gilmore G., Olszewski E. W., Niederste-Ostholt M., 2014, *MNRAS*, 437, 116  
 Bettoni D., Buson L. M., Galletta G., 2010, *A&A*, 519, A72  
 Bosma A., 1981, *AJ*, 86, 1791  
 Brosch N., Kniazev A. Y., Buckley D. A. H., O'Donoghue D., Hashimoto Y., Loaring N., Romero E., Still M., Vaisanen P., Burgh E. B., Nordsieck K., 2007, *MNRAS*, 382, 1809  
 Brosch N., Kniazev A. Y., Moiseev A., Pustilnik S. A., 2010, *MNRAS*, 401, 2067  
 Buote D. A., Jeltama T. E., Canizares C. R., Garmire G. P., 2002, *ApJ*, 577, 183  
 Burkert A., 1995, *ApJL*, 447, L25  
 Buson L. M., Bettoni D., Galletta G., 2011, *Astron. Space Sci*, 335, 231  
 Chilingarian I. V., Melchior A.-L., Zolotukhin I. Y., 2010, *MNRAS*, 405, 1409  
 Combes F., Arnaboldi M., 1996, *A&A*, 305, 763  
 Combes F., Moiseev A., Reshetnikov V., 2013, *A&A*, 554, A11  
 Cox A. L., Sparke L. S., 1996, in Skillman E. D., ed., *The Minnesota Lectures on Extragalactic Neutral Hydrogen Vol. 106 of Astronomical Society of the Pacific Conference Series*, Using HI in Polar-Ring Galaxies to Probe Galactic Potentials. p. 168  
 Cox A. L., Sparke L. S., van Moorsel G., 2006, *AJ*, 131, 828  
 Debattista V. P., Moore B., Quinn T., Kazantzidis S., Maas R., Mayer L., Read J., Stadel J., 2008, *ApJ*, 681, 1076  
 Debattista V. P., Roškar R., Valluri M., Quinn T., Moore B., Wadsley J., 2013, *MNRAS*, 434, 2971  
 Dubinski J., Carlberg R. G., 1991, *ApJ*, 378, 496  
 Dubinski J., Kuijken K., 1995, *ApJ*, 442, 492  
 Emsellem E., Cappellari M., Peletier R. F., McDermid R. M., Bacon R., Bureau M., Copin Y., Davies R. L., Krajnović D., Kuntschner H., Miller B. W., de Zeeuw P. T., 2004, *MNRAS*, 352, 721  
 Finkelman I., Moiseev A., Brosch N., Katkov I., 2011, *MNRAS*, 418, 1834  
 Franx M., van Gorkom J. H., de Zeeuw T., 1994, *ApJ*, 436, 642  
 Garbari S., Read J. I., Lake G., 2011, *MNRAS*, 416, 2318

- Gnedin O. Y., Gould A., Miralda-Escudé J., Zentner A. R., 2005, *ApJ*, 634, 344
- Hayashi E., Navarro J. F., Springel V., 2007, *MNRAS*, 377, 50
- Helmi A., 2004, *ApJL*, 610, L97
- Ibata R., Lewis G. F., Irwin M., Totten E., Quinn T., 2001, *ApJ*, 551, 294
- Iodice E., 2010, in Debattista V. P., Popescu C. C., eds, American Institute of Physics Conference Series Vol. 1240 of American Institute of Physics Conference Series, Polar Disk Galaxies as New Way to Study Galaxy Formation: the Case of NGC4650A. pp 379–382
- Iodice E., Arnaboldi M., Bournaud F., Combes F., Sparke L. S., van Driel W., Capaccioli M., 2003, *ApJ*, 585, 730
- Iodice E., Arnaboldi M., Napolitano N. R., Oosterloo T. A., Józsa G. I. G., 2008, in Funes J. G., Corsini E. M., eds, Formation and Evolution of Galaxy Disks Vol. 396 of Astronomical Society of the Pacific Conference Series, Dark Matter Content in the Polar Disk Galaxy NGC 4650A. p. 483
- Jing Y. P., Suto Y., 2002, *ApJ*, 574, 538
- Jordán A., Côté P., Blakeslee J. P., Ferrarese L., McLaughlin D. E., Mei S., Peng E. W., Tonry J. L., Merritt D., Milosavljević M., Sarazin C. L., Sivakoff G. R., West M. J., 2005, *ApJ*, 634, 1002
- Józsa G. I. G., Kenn F., Klein U., Oosterloo T. A., 2007, *A&A*, 468, 731
- Khoperskov A., Bizyaev D., Tiurina N., Butenko M., 2010, *Astronomische Nachrichten*, 331, 731
- Khoperskov A. V., Eremin M. A., Khoperskov S. A., Butenko M. A., Morozov A. G., 2012, *Astronomy Reports*, 56, 16
- Khoperskov A. V., Khoperskov S. A., Zasov A. V., Bizyaev D. V., Khrapov S. S., 2013, *MNRAS*, 431, 1230
- Khoperskov A. V., Zasov A. V., Tyurina N. V., 2003, *Astronomy Reports*, 47, 357
- Khoperskov S., Moiseev A., Khoperskov A., 2013, *Memorie della Societa Astronomica Italiana Supplementi*, 25, 51
- Krumm N., van Driel W., van Woerden H., 1985, *A&A*, 144, 202
- Kuhlen M., Diemand J., Madau P., 2007, *ApJ*, 671, 1135
- Law D. R., Majewski S. R., Johnston K. V., 2009, *ApJL*, 703, L67
- Martinsson T. P. K., Verheijen M. A. W., Westfall K. B., Bershady M. A., Andersen D. R., Swaters R. A., 2013, *A&A*, 557, A131
- Masset F. S., Bureau M., 2003, *ApJ*, 586, 152
- Moiseev A. V., 2001, *Bulletin of the Special Astrophysics Observatory*, 51, 11
- Moiseev A. V., 2008, *Astrophysical Bulletin*, 63, 201
- Moiseev A. V., Mustsevoi V. V., 2000, *Astronomy Letters*, 26, 565
- Moiseev A. V., Smirnova K. I., Smirnova A. A., Reshetnikov V. P., 2011, *MNRAS*, 418, 244
- Natarajan P., Refregier A., 2000, *ApJL*, 538, L113
- Navarro J. F., Frenk C. S., White S. D. M., 1997, *ApJ*, 490, 493
- Olling R. P., Merrifield M. R., 2000, *MNRAS*, 311, 361
- Oosterloo T., Morganti R., Crocker A., Jütte E., Cappellari M., de Zeeuw T., Krajnović D., McDermid R., Kuntschner H., Sarzi M., Weijmans A.-M., 2010, *MNRAS*, 409, 500
- Peletier R. F., Christodoulou D. M., 1993, *AJ*, 105, 1378
- Reshetnikov V., Sotnikova N., 1997, *A&A*, 325, 933
- Reshetnikov V. P., 2004, *A&A*, 416, 889
- Reshetnikov V. P., Hagen-Thorn V. A., Yakovleva V. A., 1994, *A&A*, 290, 693
- Reshetnikov V. P., Hagen-Thorn V. A., Yakovleva V. A., 1998, *Astronomy Reports*, 42, 439
- Reshetnikov V. P., Sotnikova N. Y., 2000, *Astronomy Letters*, 26, 277
- Rodionov S. A., Sotnikova N. Y., 2013, *MNRAS*, 434, 2373
- Sackett P. D., Pogge R. W., 1995, in Holt S. S., Bennett C. L., eds, Dark Matter Vol. 336 of American Institute of Physics Conference Series, Another flattened dark halo: Polar ring galaxy A0136-0801. pp 141–144
- Sackett P. D., Rix H.-W., Jarvis B. J., Freeman K. C., 1994, *ApJ*, 436, 629
- Sackett P. D., Sparke L. S., 1990, *ApJ*, 361, 408
- Schimionovich D., van Gorkom J. H., van der Hulst J. M., 2013, *AJ*, 145, 34
- Sellwood J. A., 2006, *ApJ*, 637, 567
- Sellwood J. A., Debattista V. P., 2006, *ApJ*, 639, 868
- Shapiro K. L., Gerssen J., van der Marel R. P., 2003, *AJ*, 126, 2707
- Shen J., Sellwood J. A., 2006, *MNRAS*, 370, 2
- Smirnova K. I., Moiseev A. V., 2013, *ArXiv e-prints*
- Snaith O. N., Gibson B. K., Brook C. B., Knebe A., Thacker R. J., Quinn T. R., Governato F., Tissera P. B., 2012, *MNRAS*, 425, 1967
- Sparke L. S., 2002, in Natarajan P., ed., The Shapes of Galaxies and their Dark Halos What can Polar Rings Tell us about the Shapes of Dark Matter Halos?. pp 178–185
- Sparke L. S., van Moorsel G., Schwarz U. J., Vogelaar M., 2009, *AJ*, 137, 3976
- Spavone M., Iodice E., Arnaboldi M., Gerhard O., Saglia R., Longo G., 2010, *ApJ*, 714, 1081
- Stanonik K., Platen E., Aragón-Calvo M. A., van Gorkom J. H., van de Weygaert R., van der Hulst J. M., Peebles P. J. E., 2009, *ApJL*, 696, L6
- Steiman-Cameron T. Y., Durisen R. H., 1982, *ApJL*, 263, L51
- Steiman-Cameron T. Y., Kormendy J., Durisen R. H., 1992, *AJ*, 104, 1339
- Strigari L. E., 2013, in Szczerbinska B., Babu K., Balantekin B., Dutta B., Mohapatra R. N., eds, American Institute of Physics Conference Series Vol. 1534 of American Institute of Physics Conference Series, Astrophysical interplay in dark matter searches. pp 156–164
- Theis C., Sparke L., Gallagher J., 2006, *A&A*, 446, 905
- Valenzuela O., Hernández-Toledo H., Cano-Díaz M., Puerari I., Buta R., Pichardo B., Groess R., 2013, *ArXiv e-prints*
- van der Kruit P. C., Freeman K. C., 2011, *ARA&A*, 49, 301
- van Driel W., Combes F., Casoli F., Gerin M., Nakai N., Miyaji T., Hamabe M., Sofue Y., Ichikawa T., Yoshida S., Kobayashi Y., Geng F., Minezaki T., Arimoto N., Kodama T., Goudfrooij P., Mulder P. S., Wakamatsu K., 1995, *AJ*, 109, 942
- van Uitert E., Hoekstra H., Schrabback T., Gilbank D. G., Gladders M. D., Yee H. K. C., 2012, *A&A*, 545, A71
- Vera-Ciro C., Helmi A., 2013, *ApJL*, 773, L4
- Wakamatsu K.-I., 1993, *AJ*, 105, 1745
- Whitmore B. C., Lucas R. A., McElroy D. B., Steiman-

- Cameron T. Y., Sackett P. D., Olling R. P., 1990, *AJ*, 100, 1489
- Whitmore B. C., McElroy D. B., Schweizer F., 1987, *ApJ*, 314, 439
- Zasov A. V., Khoperskov A. V., Katkov I. Y., Afanasiev V. L., Kaisin S. S., 2012, *Astrophysical Bulletin*, 67, 362
- Zasov A. V., Makarov D. I., Mikhailova E. A., 1991, *Pisma v Astronomicheskii Zhurnal*, 17, 884